Environmentally Benign Hybrid Nanocomposite Beads for Azo Dyes Remediation via Synchronized Dual Degradation Mechanisms

Faten Abou Elfadl
Egyptian Atomic Energy Authority
Hazem El-Sherif
National Research Centre
Noha Deghiedy (n_deghiedy@hotmail.com)
Egyptian Atomic Energy Authority https://orcid.org/0000-0001-6158-4079

Research Article

Keywords: Photocatalytic degradation, Reductive degradation, Metal-matrix composites, Polymer nanocomposites; Smart materials, Ionizing radiation, Textile dyeing wastewater

Posted Date: February 22nd, 2021

DOI: https://doi.org/10.21203/rs.3.rs-165839/v1

Abstract

Practically, 12% of used dyes are excluded as waste in the mobile aqueous environment. Methyl orange (MO), an industrial azo dye, is known to be carcinogenic. Accordingly, this work was engaged to fabrication of a high-efficiency visible light photocatalysts based on Ag-Alginate/Chitosan-coated MgO nanocomposite beads. MgO and Ag were prepared via precipitation and γ-radiation reduction technique as a green physical one, respectively. The degradation mechanisms depended on catalytic reduction by means of sodium borohydride/Ag and photo oxidative degradation. XRD proved the periclase crystalline form of MgO of size 20 nm and the formation of face centered cubic silver crystals of size 15 nm. The degradation yield varied directly with time, MgO and dye concentration until certain limit. Five and twenty minutes were enough to get clear solution of MO (30 and 15 ppm, respectively) while 60 min was required to achieve the same target for 60 ppm MO solution. The catalysts showed high efficiency for MO of high concentration. The incorporation of Ag into catalytic beads could support both mechanisms as it could elevate the degradation efficiency up to 50% and save the time to a great extent. Thus, this carrier fruitfully converted wastewater into an effluent that can be repaid to the water cycle with minimal strike on the ecosystem.

1. Introduction

Water, as a universal solvent, has more dissolution capability than any solvents on earth; consequently, water is exclusively vulnerable to pollution. Although water is pivotal for life, it is trashed anyhow! Man discards more than three quarters of wastewater, without being treated, into the environment; polluting watercourses of all kinds; thus, disturbing the environment and threatening the sustainability of human society. Hazardous water kills more people annually than war and violence combined. In the interim, according to Natural Resources Defense Council, our drinkable water sources are limited and fixed and less than 1% of the earth's freshwater is really easily reached to us (Landrigan et al. 2019). The practice of using dyes is perhaps the most ancient art of chemistry. Dyes from natural origins have been known before written history. Practically, 12% of used dyes are excluded as waste and ~ 20% of this wastage passes to the environment, taking into account the mobility of water systems in the environment. Consequently, dye removal has occupied a noticeable position in both research and industry (Viswanathan 2018). The most plentiful compounds (60–70%) in textile wastes are azo dyes (Lellis et al. 2019). Methyl orange "MO", an azo dye, which is broadly employed in numerous industries, is recognized as carcinogenic and mutagenic. Accordingly, the degradation of MO has drawn specific attention since the last decade and up-to-the-minute (Homaeigohar 2020).Until now, a variety of strategies have been invented to treat wastewater including chemical or physical coagulation and/or flocculation (Rajasulochana and Preethy 2016); sedimentation (Conserva et al. 2019); adsorption (Zha et al. 2018), membrane filtration (Couto et al. 2018) and biological degradation method (Joss et al. 2006).

Now more than ever, the advanced oxidation processes (AOPs), defined as near-ambient temperature processes that include the creation of extremely reactive radical intermediates, particularly the hydroxyl

e non-biodegradable and highly stable

compounds in water (Oturan and Aaron 2014). The ˙OH radicals are strong and non-selective oxidants and react positively with most of the organic compounds (Cuerda-Correa et al. 2020). Also, no hazards will be produced due to the end products of the AOPs being just CO_2, H_2O, or small inorganic ions. Actually, the core of AOPs relies on the light radiation on the photocatalysts to motivate the oxidization reaction, and during the whole reaction process, no extra energy is required; consequently, it is chemically a green technique (Ameta and Ameta 2018).

However, in terms of the relatively low photocatalytic efficiency, the practical use of the photocatalysts remains limited (Ge et al. 2019). Problematic photo-corrosion issues, in aqueous media, via redox reactions and the fast recombination of electron-hole pairs are severe attributes of newly developed visible light response semiconductors (Cuerda-Correa et al. 2020; Ge et al. 2019; Martini et al. 2019). The slowness and the energy consumption are additional aspects of these processes. Quite the reverse, catalytic reduction is a comparatively faster process. Catalytic reductive degradation of organic dye molecules, by $NaBH_4$ “NBH” in front of metal nano particles (MNPs), takes place by an electron transfer process. MNPs could reduce the activation energy; thus, making the process kinetically feasible (Saikia et al. 2017). NBH is moderately mild reducing agent, mostly employed for the reduction of reactive functional groups in protic solvents. Nonetheless, the rate of reduction is often slow (Zeynizadeh and Behya 2005) and does not meet the requirements for approval of this technology in the treatment of wastewater.

Being a heterogeneous catalyst, MgO is environmentally benign, non-corrosive, has high thermal stability and presents less disposal difficulties (Almerindo et al. 2011). What's more, nanomaterial MgO expresses smaller size, greater surface area and attractive quantum related properties which are wholly different from bulk one. Therefore, it can display fantastic efficiency for diverse applications (Saravanan et al. 2016). For instance, nano-sized MgO was outstanding basic catalyst for several organic reactions (Riyadh et al. 2018). Large band gap, low dielectric constant and its refractive index are the main criteria that have generated many attempts to employ MgO as a photocatalyst for dyes degradation in aqueous solution (Zheng et al. 2019). However, stabilization is a significant issue in nanoparticles synthesis; where the particles tend to agglomerate; increase in size with subsequent flocculation. Fortunately, this can be avoided by the use of a good stabilizer like polymers; since they allow better particle size control. Polysaccharides have also been used for this purpose such as chitosan and its derivatives, due to their excellent synergy and bifunctional expected effects (León et al. 2017). Besides, the main problems to the prospective use of MgO NPs as catalysts are their challenging separation and reusability as the exploited catalyst could not be recovered quantitatively and the pure products should be obtained after far-reaching purification procedures (Riyadh et al. 2018; Zheng et al. 2019). Consequently, incorporation of these NPs into beads may be a must to overcome these challenges. For instance, alginate, a hydrophilic, biocompatible and inexpensive biopolymer, is one of the most broadly used biopolymer for eliminating the anionic and cationic pollutants from aqueous solutions and conveniently, an inter-connected open pore network can be formed via divalent ions cross-linking like calcium ions (Asadi et al. 2018).

Likewise, silver NPs also display significant UV light absorption due to the transition of 4*d* electrons to the 5*sp* band. Consequently, silver NPs are potentially photocatalysts that make use of the full solar spectrum. Silver NPs on the surface of semiconductors/electron-donor substances lead to charge separation between photo-generated electron-hole pairs, thus improving the whole photocatalytic activity (Chen et al. 2010). As it remains a significant challenge, the approach proposed in this work is very simple, but allows overcoming the aforementioned difficulties and benefits from the advantages of both catalytic reduction and photodegradation mechanisms and MgO NPS along with Ag NPs. We assumed that Ag NPs can augment both mechanisms of dye degradation and both routes can complement each other to achieve better results, regarding saving of time and energy.

For that reason, our work has been engaged, for the first time as far as we are aware, with fabrication of a high-efficiency visible light photocatalyst established on orchestrated mechanisms of simultaneous photo oxidative and catalytic reductive degradation. Ag-Alginate/Chitosan-coated MgO nanocomposite beads were synthesized. The reduction of Ag^{+} to silver NPs was achieved via γ-radiation reduction technique as a green physical one. This synchronized dual catalyst could give a fascinating efficiency as it could degrade 30 ppm MO solution in about 5 min under visible light.

2. Experimental Section

2.1 Materials

Alginic acid sodium salt (Na-ALG) from brown algae, of MW = 90-180 kDa and M/G= 65/35, was purchased from Sigma-Aldrich, USA. Calcium chloride dihydrate ($CaCl_2.2H_2O$) was purchased from Algomhoria Co., Egypt. Chitosan (MW 300,000), silver nitrate $AgNO_3$ and magnesium nitrate hexahydrate ($Mg(NO_3)_2.6H_2O$) were purchased from Acros Organics, United Kingdom. Sodium hydroxide (NaOH) was got from ADWIC Co., Egypt. Double distilled water was used throughout the study. All reagents were of analytical grade and were used as received without further purification.

2.2. Preparation of MgO coated with chitosan

First of all, a chitosan solution was prepared by stirring 1% wt./vol. of chitosan into 1% acetic acid solution overnight until complete dissolution. Under vigorous stirring, 100 ml of 1M magnesium nitrate was added until a clear homogeneous solution was attained and at that point, 100 ml of 0.5M sodium hydroxide solution was added drop wisely. For instance, a white suspension rapidly started to appear. The formed suspension was left to settle and then the precipitate was washed several times with distilled water to remove excess sodium hydroxide; filtered and calcined at 450°C for 4h. The resulted powder was grinded and stored in sealed polyethylene bag until usage.

2.3. Preparation of alginate/MgO/chitosan beads

Different concentrations, namely, 1%, 3%, and 5% of MgO/CS aqueous dispersion were added in separate e solution and mixed well with magnetic stirrer

until being homogeneous. By using a 10 ml syringe, ALG/(MgO/CS) mixtures were added drop wisely into a 3% wt./vol. solution of $CaCl_2.2H_2O$ under magnetic stirring. Although nanocomposite beads were formed instantly, the gelation reaction was permitted to continue for more than 8 hours to ensure complete gelation. Finally, the beads were rinsed gently with distilled water and dried at 37°C. The synthesized beads are named henceforth as ALG-(MgO/CS) beads.

2.4. Radiation of silver ions-containing alginate/MgO/chitosan nanocomposite beads

First, 50 ml of 0.2% silver nitrate solution was added to 25 ml of the as-synthesized beads dispersion containing 5% MgO. And then, the beads were exposed to γ-radiation to start the reduction of silver ions to silver nanoparticles. The formed nanocomposite beads, named hereafter as Ag/ALG-(MgO/CS), were then removed and washed thoroughly with distilled water, using stainless steel grid and left to dry at room temperature. γ-radiation was achieved at the National Center for Radiation Research and Technology (NCRRT), Egyptian Atomic Energy Authority. The irradiation process was implemented by ^{60}Co facility for a total dose of 50 kGy and at dose rate 1.7 Gy h^{-1}.

2.5. Characterization of alginate based catalytic beads

The successful formation of MgO NPs was realized by Energy-dispersive X-ray (EDX) spectroscopy linked with the scanning electron microscope (JEOL SEM- 5400, Japan). The size and size distribution of MgO NPs in the colloids were measured by means of dynamic light scattering (DLS) technique via PSSNICOMP Zeta Potential/Particle Sizer 380ZLS (PSS-NICOMP, Santa Barbara, CA, USA). The measure of the size distribution breadth polydispersity index (PDI) was also reported. The sample was loaded into quartz micro-cuvette. Five measurements were made at room temperature and the mean result was recorded. Fourier transforms infrared spectrometer (FT-IR) spectra were recorded in KBr dispersion in the range of 400 to 4000 cm^{-1}, using a Bruker Vertex 70 FTIR spectrometer, Germany, at resolution of 4 cm^{-1}. X-ray diffraction (XRD) analysis was executed by a Shimadzu instrument (XRD-6000 series, Japan) with Cu-Kα radiation (λ = 1.54 Å), operated at 40 kV and 30 mA. XRD patterns were recorded in the range of 2θ = 4-90° (by steps of 0.02°). The pore sizes and the morphology of the dry beads were determined from the SEM images taken by JEOL-T20, Japan.

2.6. Evaluation of Photocatalytic activity

The nano-hybrid beads were engaged for exploring the degradation of MO using $NaBH_4$ as the reducing agent. The reaction was achieved in aqueous medium at 30±1°C. The degradation process was assessed by UV-Vis spectrophotometer (Shimadzu UV-2600 spectrophotometer against the standard calibration curve for MO at λ_{max} = 480 nm) through the decrease of respective absorbance maxima. In a specific reaction procedure, 30 mL of aqueous dye solution was added to 2mL of 0.2M $NaBH_4$. Then, definite amount of the nano-hybrid beads, namely, 1; 3 and 5%, was supplemented into the dye solution (15; 30 and 60 ppm) and the whole mixture was stirred. At certain intervals of time, an aliquot of the solution was

transferred to a quartz cuvette and its UV-Vis absorbance spectrum was noted. The efficiency of dye degradation (%) was calculated as follows:

$$\textbf{Degradation Efficiency} = \frac{A_o - A_t}{A_o} x100$$

where, A_o is the initial absorbance of dye solution and A_t is the absorbance at certain time (t).

2.7. Statistical analysis

All tests were replicated at least five times and the mean value was calculated to ensure the data reproducibility and to judge the precision of the recorded data.

3. Results And Discussion

3.1. Synthesis of MgO NPs and Ag/ALG-(MgO/CS) nanocomposite beads

Magnesium oxide nanoparticles (MgO NPs) were synthesized by the simple and economical precipitation method to achieve homogeneous coverage of MgO with chitosan chains. Chitosan and alginate are natural polymers that have been used comprehensively since few decades; due to accessibility, low cost, biodegradability and biocompatibility (Mikula et al. 2019). Chitosan is a linear polysaccharide, in which β-(1–4) glycosidic bonds are the linkages among D-glucosamine and N-acetyl-D-glucosamine units. Theoretical and experimental information have demonstrated that chitosan and metals ions form coordination bonds. The metal ion (Mg^{2+}) is bonded to an amino group of chitosan and coordinated with several amino groups in the same polymer or different polymers of chitosan (León et al. 2017) as shown in Fig. 1. As a general rule, metal NPs aggregate together and gradually grow into greater clusters and finally precipitate. Thus, nanoscale deviation is predictable. This evades the usefulness of synthesized NPs and dampens its application. A cluster stabilizer, e.g. chitosan, may prevent such coalescence (Van Phu et al. 2014). Any remaining chitosan after the calcination step could degrade into fragments under gamma irradiation during the reduction of $AgNO_3$.

Alginate (ALG), has a particular shape of both its monomers and their linkage; as it is composed of 1,4'-β-d-mannuronic acid (M-block) and α-l-guluronic acid (G-block). The first denotes to an extended ribbon and the latter has buckled structure. A diamond shaped hole is the outcome of side by side two G-block arrangement. The dimensions of this hole are perfect for cooperative binding of divalent cations like calcium ions. Calcium can right fit into the guluronate structures similar to eggs in an egg-box. Accordingly, the alginate chains bind together by junction zones and this ionotropic interaction produces gels with interconnected pores structure (Segale et al. 2016; Ching et al. 2017) as shown in Fig. 2.

In a valuable study, Lee et al. (2010) compared between the in-situ reduction and γ-irradiation methods and they recorded more stability and lower average size of Ag NPs prepared by the former. Silver ions "Ag^{+}" can be reduced by chemical, electrochemical and photochemical reduction as well as thermal, ultrasound, microwave and electron irradiation. While, chemical methods of synthesizing Ag NPs are artless compared with physical methods, the former have more than a few drawbacks over the latter; as a residual reducing agents may associate with the environment causes many eco-problems. For that reason, maturing of a green method to synthesize Ag NPs is anticipated and looked-for (Van Phu et al. 2014).

Gamma irradiation creates solvated electron which reacts very quickly with NO_3^- obtained from $AgNO_3$. Oxidative and reductive species, generated by radiolysis of water, react in competition with Ag^+ and NO_3^- inside the beads producing Ag NPs (He et al. 2015) as presented in Fig. 3. In this figure, the scheme illustrates that reduction of Ag^+ can be achieved via the hydrated electrons e^-_{aq}. The neutral atom Ag^0 reacts with Ag^+ to form quite stabilized Ag clusters. Finally, such clusters arrange together or absorb neutral Ag^0 in order to form the Ag NPs (Van Phu et al. 2014; Chen et al. 2007).

3.2. Characterization of synthesized MgO NPs and ALG-based beads

3.2.1. DLS and EDX analysis of as-synthesized MgO NPs

The Dynamic Light Scattering (DLS) is a technique currently used for measuring particle size over a size range from nanometers to microns. Figure 4 shows the DLS and EDX spectrum of the as-synthesized MgO NPs. The size distribution is symmetric, displaying that data near the mean are more frequent in occurrence i.e. Gaussian distribution which could prove the size uniformity of MgO NPs. The mean particle diameter of MgO NPs was $\approx$ 16.7 nm which was in line with that calculated by XRD. The inset image of Fig. 4 illustrates the elemental composition of the MgO NPs as determined via EDX spectrum. The recorded atomic percentage of Mg was 100.00%. Thus, confirms the efficient synthesis procedure of pure MgO nanoparticles.

3.2.2. XRD analysis

In order to investigate the structural properties of the nanocomposite beads, XRD was employed. Figure 5 displays the graph of intensity against angular position to designate the XRD pattern of synthesized ALG-(MgO/CS) and Ag/ALG-(MgO-CS) beads. For ALG-(MgO/CS) pattern, it is worth mentioning that (JCPDS Card No.: 75-1525) refers to periclase crystalline form of MgO. Accordingly, the peak positions at 2θ = 31.34°, 36.78°, 42.73°, 45.08° and 62.17° were devoted to this crystalline form. Any other crystalline phase was not identified in XRD pattern of synthesized MgO NPs. The calculated mean crystallite size of MgO NPs, using Debye–Scherrer formula was approximately 20 nm. For Ag/ALG-(MgO/CS), in view of JCPDS (Card No.: 89-3722), XRD points out that the peaks at 38.17°, 44.28°, 64.5°, 77.52° and 81.62° could be recognized as 111, 200, 220, and 311 crystallographic planes of the face centered cubic silver crystals, respectively (Anandalakshmi et al. 2016). Furthermore, the principal crystalline phase was silver;

no noticeable impurities (e.g., Ag_2O) were recognized in the XRD patterns. The mean particle size of Ag NPs was around 15 nm.

3.2.3. Surface morphology analysis

Representative scanning electron microscopy (SEM) micrographs of the ALG-(MgO/CS) and Ag/ALG-(MgO/CS) nanocomposite beads, with different magnifications, are presented in Fig. 6. The SEM image, of ALG-(MgO/CS), as shown in Fig. 6a, reveals that dry alginate beads were spheres of porous surface and micrometrical size. Figure 6b displays a 3-D interconnected large pore structure with different size. The pore size and the interconnected zones may depend on $CaCl_2$ concentration as a crosslinker. The images also confirm the even distribution of MgO particles through alginate beads.

While reduction of $AgNO_3$, inside the beads by γ-radiation, resulted in low irregularities in bead spherical shape, as shown in Fig. 6c, the radiation process could not deform the spherical beads morphology. Also, it can be seen that silver atoms were thoroughly distributed into the beads. However, the microporous structure was damaged and noticeable surface changes could be remarked [Fig. 6d].

3.2.4. FTIR Analysis

Figure 7 displays the graphs of transmittance versus wavenumber derived from FTIR analysis of ALG, ALG-(MgO/CS) and Ag/ALG-(MgO/CS). In ALG spectrum, the hydroxyl groups at 3255 cm^{-1}, asymmetric carboxyl at 1645 cm^{-1}, (-CH) at 1420 cm^{-1} and (C-O-C) at 1025 cm^{-1} are endorsed to the major functional groups of sodium alginate. In ALG-(MgO/CS) spectrum, the cross-linking slightly reduced the wavenumber of the carboxyl band from 1645 to 1598 cm^{-1}, (-CH) from 1420 to 1408 cm^{-1} and bands of (C-O-C) from 1025 cm^{-1} to 1022 cm^{-1}.

Mg-O stretching vibrational band at 540 cm^{-1} could not be perceived in the spectrum of nanocomposite; as these bands overlap significantly with the intense bands of ALG as seen in ALG-(MgO/CS) spectrum. Also, the presence of functional groups of ALG approves that MgO NPs did not influence the structural integrity of this natural polymer. The FTIR spectrum of Ag/ALG-(MgO/CS) composite reveals a significant shift from 1598 to 1620 cm^{-1} due to the asymmetric stretching of –COO – metal groups. This shift verifies the interaction between alginate (carboxylate) and Ag NPs. Moreover, the shift of the band from 1420 to 1394 cm^{-1} may indicate that ALG was doped by NO_3^- and hence the stabilization of Ag-NPs by the –COO – group of ALG could occur (Wang et al. 2016). Of note, the peak attributed to vibration of Ag–Ag metallic bonds cannot be observed in this graph; since the employed mid-infrared ray (4000–400 cm^{-1}) is not appropriate to measure such vibration (Gharibshahi et al. 2017). The comparison of FTIR spectra between the ALG-(MgO/CS) and Ag/ALG-(MgO/CS) shows only minor changes in the absorption bands. The band shift in the range of 3200–3500 cm^{-1} was not remarkable, but the decrease in intensity was sharp. From such shifting and decreasing bands intensities in FT-IR bands, it may be concluded that there was an interaction mechanism between ALG and Ag-NPs, for instance, Ag-NPs may be capped by the ion pair electrons around oxygen atoms in ALG via van der Waals interactions.

3.3. Photocatalytic activity of ALG-(MgO/CS) and Ag/ALG-(MgO/CS) beads

Severe water contamination and drainage of fossil resources have come to be vital and critical global issues yet to be solved. Photocatalytic routes, established via solar energy and semiconductor catalysts, are believed as the most optimistic techniques for wastewater remediation. The visible light is about 43% of solar energy; therefore, the development of a visible light catalyst is particularly a vital topic (Ge et al. 2019). In the following section, the evaluation of the as-synthesized beads, as visible light catalysts, will be given.

3.3.1. Influence of MgO content in ALG-(MgO/CS) beads on their catalytic activity

Figures 8 (a-c) elucidates the relation between the degradation efficiency of ALG-(MgO/CS) beads and time through different MO concentration, namely, 15, 30 and 60 ppm and the study parameter was MgO percentages. By perceiving these figures, it may be alleged that increasing the concentration of MgO from 1 to 5% visibly promotes the degradation efficiency. This observation has invariably been recorded in literature as the rate growths with catalyst loading but till definite time above which, the rate of dye degradation slightly decreases with time; as there can be a saturation point beyond which, the solid amount (of dye) could not have a direct correlation to the degradation magnitude (Viswanathan 2018). Moreover, the efficiency is correlated with dye concentration as it varied from 71% to 85% and finally to 32% for 15, 30 and 60 ppm MO, respectively, at 60 min and for 5% MgO containing catalyst. These results may be rationalized in terms of adsorption. As the rate of the dye decomposition rests on both the adsorption equilibrium that occurs on the surface and the adsorbed concentration; the solid weight possibly point to the saturation limit of dye adsorption and perhaps restricts the amount of the dye solution that can be engaged with degradation (Viswanathan 2018). Although adsorption is a mandatory for photocatalysis and more adsorption would result in more photocatalysis, the penetration of light, through higher concentration of dye solution, suffers considered difficulties (Raliya et al. 2017). Besides, as the MO concentration increased, the observed lower reaction rate may be owing to blocking of MO of high concentration to light interaction with the photocatalyst surface. Therefore, a lower Figures 8 (a-c) elucidates the relation between the degradation efficiency of ALG-(MgO/CS) beads and time through different MO concentration, namely, 15, 30 and 60 ppm and the study parameter was MgO percentages. By perceiving these figures, it may be alleged that increasing the concentration of MgO from 1 to 5% visibly promotes the degradation efficiency. This observation has invariably been recorded in literature as the rate growths with catalyst loading but till definite time above which, the rate of dye degradation slightly decreases with time; as there can be a saturation point beyond which, the solid amount (of dye) could not have a direct correlation to the degradation magnitude (Viswanathan 2018). Moreover, the efficiency is correlated with dye concentration as it varied from 71% to 85% and finally to 32% for 15, 30 and 60 ppm MO, respectively, at 60 min and for 5% MgO containing catalyst. These results may be rationalized in terms of adsorption. As the rate of the dye decomposition rests on both the adsorption equilibrium that occurs on the surface and the adsorbed concentration; the solid weight possibly point to the saturation limit of dye adsorption and perhaps restricts the amount of the dye solution that can be engaged with degradation (Viswanathan 2018). Although adsorption is a mandatory for photocatalysis , the penetration of light, through higher

concentration of dye solution, suffers considered difficulties (Raliya et al. 2017). Besides, as the MO concentration increased, the observed lower reaction rate may be owing to blocking of MO of high concentration to light interaction with the photocatalyst surface. Therefore, a lower

3.3.2. Impact of silver on ALG-(MgO/CS) beads on highly concentrated dye

Employing nanotechnology into dye degradation domain shows great prospective, as nanoparticles can react with dyes chemically; producing non-toxic products that may not require removal (Viswanathan 2018). For instance, Ag NPs play an important role in the improvement of photocatalytic performance for the organic dyes' degradation (Wu et al. 2017). For that reason and to treat relatively poor efficacy of catalysts at high concentration level of dye (49% at equilibrium for 60 ppm MO and 5% MgO), we proved the positive influence of Ag NPs on the as-synthesized catalyst. Figure 9 illustrates the impact of Ag NPs on the ALG-(MgO/CS) by studying the equilibrium degradation of 60 ppm MO via increasing MgO content from 1 to 5%, then by incorporating Ag NPs into constant weight catalysts (0.5g, containing 5% MgO).

The last bar in this figure denotes to insertion of Ag NPs in the beads. At first glance, Ag NPs gave fascinating results as these particles enhanced the degradation efficiency to about 99%. The up-grading in catalyst efficiency was about 50%, which may be attributed to strong absorption of visible light by Ag NPs due to the so called surface plasmon resonance "SPR" that can be explained in terms of resonance of electrons. This resonance, between conduction band electrons of nanoparticles and the oscillating electric field of incident light, can create plasmonic excited electrons that can discharge heat to the lattice once they return to their thermal equilibrium states. This can make and prompt reactions of molecules adsorbed on the particles. It is worthy to know that visible light absorption can make this resonance i.e. heat and promote electrons to higher energy levels; encouraging their contribution to chemical reactions, especially those involve electron transfer (Chen et al. 2010).

2.3.3. Optimization of catalyst weight of Ag/ALG-(MgO/CS) beads

By altering the catalyst weight at 60 ppm MO concentration, as seen in Fig. 10, it can be noticed that the degradation efficiency was reduced only about 5% in case of decreasing catalyst weight from 0.5 to 0.1 g. The figure proves the ability of nano silver to enhance the catalyst efficiency. This can be attributed to one or more of the following reasons: easily excited electron-hole pairs; the higher absorption ability of catalyst to photons could led to more electron-hole pairs; higher quantum efficiency of the photo-generated electron-hole pairs caused by inhibition of their recombination; the more reaction sites by reason of large surface area of the catalysts; and the favorable stable chemical and physical structures of photocatalysts that could facilitate the mass transfer in water (Ge et al. 2019).

3.3.4. Monitoring the photocatalytic activity Ag/ALG-(MgO/CS) beads

In order to give other practical evidence of Ag imposed efficiency, the current study monitored the degradation of MO with time as shown in Fig. 11. It can be observed that five and twenty minutes were enough to get clear solution of the dye (30 and 15 ppm, respectively as shown in the inset) while 60 min was required to achieve the same target for 60 ppm MO solution as both pseudo first order rate (not

studied here) and degradation extent decreased markedly with the increase in the initial dye concentration (Liu et al. 2015).

This promoted efficiency may be due to, besides SPR discussed above, the higher collision frequency and consequently the probability for the bombardment of incoming photons with the dye molecules at the active sites on the surface of the catalyst. As a consequence, the catalytic activity was mainly originated from the photo generated charges created by Ag NPs. Ag in the photocatalysts exists as Ag^0, which is different from its salts which can provide electrons and display photocatalytic activity via ions oxidation of by means of light irradiation. The photocatalytic reactions (degradation and selective oxidation) encompass electron transfer from the molecules of the oxidized reactant to those of the reduced one. Thus, we accept as true that the Ag NPs initiate and facilitate the electron transfer for the photooxidation reactions (Chen et al., 2010).

By looking through the literature, it may be concluded that the slow rate of the photocatalytic oxidation reactions was remarkable. In a previous study, a polytetrafluoroethylene-Al based triboelectric nanogenerator (TENG) whose electric power output was utilized to clarify solution of 20 mg l^{-1} MO; using UV, the degradation (%) of MO were 76 and 27% in 120 min, with and without TENG assistance, respectively (Su et al. 2013) and in a recent study [38], the aqueous solution of MO, oxidized by H_2O_2 catalyzed by Silica-PI L-Au, was clarified after 16 h. What is more, after 420 min of UV irradiation using 0.6 g/l TiO_2, the MO degradation was up to 97% and the absorption peak was entirely removed (Su et al. 2013). Besides, Raliya et al. (2017) attributed the removal a total of 40% of the dye in 120 min, utilizing 25nm ZnO under visible light conditions, to the high surface area/volume ratio of the small particles.

It is important to shed light on this impressive current data, this can be performed by the comparison infographic shown in Fig. 12, to visualize our data and weigh aspects of each catalyst. Our results coincide with Saikia et al. (2017) that unaided $NaBH_4$ could not reduce the dye even after 90 min; due to a large difference in redox potential between the electron donor (borohydride ion) and acceptor (dyes) species, which can hinder electrons relaying. Due to their high electron relaying capability, Ag NPs could enhance the catalytic reduction of borohydride. In terms of MgO photocatalytic activity, the enhanced activity may be recognized on the basis that fewer electrons are expected to return to the valence band once excited, leading to less energy loss and relatively higher dye degradation efficacy (Raliya et al. 2017).

Although the current data confirmed that the noble metal, like Ag NPs, has been capable of achieving a marvelous significance in catalytic dye degradation; since their worthy electron relaying capability originates from their apt redox potentials, there is an apparent contradiction with Chen et al. (2010) who suggested that under irradiation of moderate intense visible light, an insignificant number of silver electrons, at high temperature, gains appropriate energy to be captured by O_2 molecules. As a result, a weak surface photocurrent signal and slow dye degradation were recorded. This deceptive contradiction may be solved by the fact that the photocatalytic activity of the Ag NPs themselves has not been realized;

Ps on the surface of semiconductors and

electron-donor substances lead to charge separation of photo generated electron-hole pairs and as a consequence, augmenting the overall photocatalytic activity. Thus, Ag NPs could promote both mechanisms of dye degradation.

Thus, our results can be considered inspiring regarding time and energy saving; probably due to the dual effect of the catalyst as reductive, in the presence of $Ag/NaBH_4$ and oxidative, in the presence of Ag/MgO/visible light.

3. Conclusion

Research in certain arenas of science is restricted to definite regions of the world; however, the degradation of dyes has been investigated in almost all the countries. Accordingly, this work was engaged to fabrication of a high-efficiency visible light photocatalyst based on Ag/ALG-(MgO/CS) nanocomposite beads. The degradation mechanisms depended on two mechanisms, namely, catalytic reduction in the presence of $Ag/NaBH_4$ and photo oxidative degradation due to Ag/MgO, employing visible light irradiation. Utilizing ALG-(MgO/CS) beads, the photocatalytic degradation was being correlated with dye concentration as it varied, after an hour, from 71% to 85% and finally to 32% for 15, 30 and 60 ppm MO, respectively. The study proved the positive impact of Ag NPs on MgO photocatalyst as the former could alter both the saturation level and increase the degradation efficiency (rate). Five and twenty minutes were enough to get clear solution of the dye (30 and 15 ppm, respectively) while 60 min was required to achieve the same target for 60 ppm MO solution. Our results confirmed that Ag NPs have been able to gain marvelous significance in catalytic dye degradation, especially for highly concentrated dye, as the results showed 50% promotion in catalyst efficiency. Thus, Ag NPs could promote both applied mechanisms of dye degradation. There is no such an entity as an exclusively benign, but it is crucial to be cautious of waste formation/removal, energy consumption, safety and time. The dual action of the catalyst has been proved to save both time and energy. The new photocatalysts will permit usage of visible light, the plentiful green energy source; to motivate beneficial chemical reactions; this will relieve our dependence on fossil fuel energy and lessen energy depletion and CO_2 emissions. Finally, in most of the studies reported, details of adsorption of the dye and its impact on the degradation kinetics have not been interrelated yet. This linking will necessary be studied in the future, for approval of such technology in the treatment of wastewater. Also, up to the present time even the detailed and thorough nature of the reaction mechanism, for the catalysis involving plasmonic silver, has not been elucidated. Furthermore, it remains a substantial challenge that deserves rational confrontation, to design an extraordinary efficient visible light photocatalyst exclusively based on a single semiconductor.

Declarations

Authors' contributions

Faten I. Abou Elfadl: Investigation, Validation, Writing - Review & Editing. **Hazem M. El-Sherif**: [illegible]inal Draft. **Noha M. Deghiedy:** Methodology,

Investigation, Visualization, Writing - Review & Editing. All authors read and approved the final manuscript.

Conflict of Interests

The authors declare that they have no known competing financial interests or personal relationships that could have appeared to influence the work reported in this paper.

Funding

This research did not receive any specific grant from funding agencies in the public, commercial, or not-for-profit sectors.

Data availability

The raw/processed data required to reproduce these findings can be shared by the authors upon request.

Compliance with ethical standards:

Competing interests: The authors declare that they have no competing interests.

Ethical approval: Not applicable.

Consent to participate: Not applicable.

Consent to publish: Not applicable.

References

Almerindo GI, Probst LF, Campos CE, De Almeida RM, Meneghetti SM, Meneghetti MR, Clacens JM, Fajardo HV (2011) Magnesium oxide prepared via metal–chitosan complexation method: Application as catalyst for transesterification of soybean oil and catalyst deactivation studies. J Power Sour 196: 8057-8063. https://doi.org/10.1016/j.jpowsour.2011.05.030

Ameta SC, Ameta R (2018) Advanced oxidation processes for wastewater treatment: emerging green chemical technology. Academic Press,UK.

Anandalakshmi K, Venugobal J, Ramasamy V (2016) Characterization of silver nanoparticles by green synthesis method using Pedalium murex leaf extract and their antibacterial activity. Appl Nanosci 6:399-408. https://doi.org/10.1007/s13204-015-0449-z

Asadi S, Eris S, Azizian S (2018) Alginate-based hydrogel beads as a biocompatible and efficient adsorbent for dye removal from aqueous solutions. ACS Omega 3:15140-15148. https://doi.org/10.1021/acsomega.8b02498

Chen P, Song L, Liu Y, Fang YE (2007) Synthesis of silver nanoparticles by γ-ray irradiation in acetic water solution containing chitosan. Radiat Phys Chem 76:1165-1168. https://doi.org/10.1016/j.radphyschem.2006.11.012

Chen X, Zheng Z, Ke X, Jaatinen E, Xie T, Wang D, Guo C, Zhao J, Zhu H (2010) Supported silver nanoparticles as photocatalysts under ultraviolet and visible light irradiation. Green Chem 12:414-419. https://doi.org/10.1039/B921696K

Ching SH, Bansal N, Bhandari B (2017) Alginate gel particles–A review of production techniques and physical properties. Crit Rev Food Sci Nutr, 57:1133-1152. doi: 10.1080/10408398.2014.965773

Conserva S, Tatti F, Torretta V, Ferronato N, Viotti P (2019) An integrated approach to the biological reactor–sedimentation tank system. Resour 8:94-113. https://doi.org/10.3390/resources8020094

Couto CF, Lange LC, Amaral MC (2018) A critical review on membrane separation processes applied to remove pharmaceutically active compounds from water and wastewater. J Water Process Eng 26:156-175. https://doi.org/10.1016/j.jwpe.2018.10.010

Cuerda-Correa EM, Alexandre-Franco MF, Fernández-González C (2020) Advanced oxidation processes for the removal of antibiotics from water. An overview. Water 12:102-153. https://doi.org/10.3390/w12010102

Faried M, Shameli K, Miyake M, Hajalilou A, Zamanian A, Zakaria Z, Abouzari-Lotf E, Hara H, Khairudin NBA, Nordin MFBM (2016) A green approach for the synthesis of silver nanoparticles using ultrasonic radiation's times in sodium alginate media: characterization and antibacterial evaluation. J Nanomater 2016:4941231. https://doi.org/10.1155/2016/4941231

Ge J, Zhang Y, Heo YJ, Park, SJ (2019) Advanced design and synthesis of composite photocatalysts for the remediation of wastewater: A review. Catal 9:122-154. https://doi.org/10.3390/catal9020122

Gharibshahi L, Saion E, Gharibshahi E, Shaari AH, Matori KA (2017) Structural and optical properties of Ag nanoparticles synthesized by thermal treatment method. Mater 10:402-415. doi: 10.3390/ma10040402

He L, Dumée LF, Liu D, Velleman L, She F, Banos C, Davies JB, Kong L (2015) Silver nanoparticles prepared by gamma irradiation across metal–organic framework templates. RSC Adv 5:10707-10715. https://doi.org/10.1039/C4RA10260F

Homaeigohar S (2020) The nanosized dye adsorbents for water treatment. Nanomater 10:295-338. doi: 10.3390/nano10020295

Joss A, Zabczynski S, Göbel A, Hoffmann B, Löffler D, McArdell CS, Ternes TA, Thomsen A, Siegrist H (2006) Biological degradation of pharmaceuticals in municipal wastewater treatment: proposing a org/10.1016/j.watres.2006.02.014

Landrigan PJ, Fuller R, Acosta NJ, Adeyi O, Arnold R, Baldé AB, Bertollini R, Bose-O'Reilly S, Boufford JI, Breysse PN, Chiles T (2018) The Lancet Commission on pollution and health. Lancet 391: 462-512. doi: 10.1016/S0140-6736(17)32345-0

Lee CJ, Karim MR, Vasudevan T, Kim HJ, Raushan K, Jung MJ, Kim DY, Lee MS (2010) A comparison method of silver nanoparticles prepared by the gamma irradiation and in situ reduction methods. Bull Korean Chem Soc 31:1993-1996. https://doi.org/10.5012/bkcs.2010.31.7.1993

Lellis B, Fávaro-Polonio CZ, Pamphile JA, Polonio JC (2019) Effects of textile dyes on health and the environment and bioremediation potential of living organisms. Biotechnol Res Inn 3:275-290. https://doi.org/10.1016/j.biori.2019.09.001

León Y, Cárdenas G, Arias M (2017) synthesis and characterizations of metallic nanoparticles in chitosan by chemical reduction. J Chil Chem Soc 62:3760-3764. http://dx.doi.org/10.4067/s0717-97070170004037 60

Liu X, Yang Y, Shi X, Li K. (2015) Fast photocatalytic degradation of methylene blue dye using a low-power diode laser. J Hazard Mater 283:267-75. doi:10.1016/j.jhazmat.2014.09.031

Martini J, Orge CA, Faria JL, Pereira MF, Soares O (2019) Catalytic advanced oxidation processes for sulfamethoxazole degradation. Appl Sci 9:2652-2670. https://doi.org/10.3390/app9132652

Mikula K, Skrzypczak D, Ligas B, Witek-Krowiak A (2019) Preparation of hydrogel composites using Ca^{2+} and Cu^{2+} ions as crosslinking agents. SN Appl Sci 1:643-658. https://doi.org/10.1007/s42452-019-0657-3

Oturan MA, Aaron JJ (2014) Advanced oxidation processes in water/wastewater treatment: principles and applications. A review. Crit Rev Env Sci Technol 44:2577-2641. https://doi.org/10.1080/10643389.2013.829765

Rajasulochana P, Preethy V (2016) Comparison on efficiency of various techniques in treatment of waste and sewage water–A comprehensive review. Resour Eff Technol 2:175-184. https://doi.org/10.1016/j.reffit.2016.09.004

Raliya R, Avery C, Chakrabarti S, Biswas P (2017) Photocatalytic degradation of methyl orange dye by pristine titanium dioxide, zinc oxide, and graphene oxide nanostructures and their composites under visible light irradiation. Appl Nanosci 7:253-259. https://doi.org/10.1007/s13204-017-0565-z

Riyadh SM, Khalil KD, Aljuhani A (2018) Chitosan-MgO nanocomposite: one pot preparation and its utility as an ecofriendly biocatalyst in the synthesis of thiazoles and [1, 3, 4] thiadiazoles. Nanomater 8:928-938. doi: 10.3390/nano8110928

Saikia P, Miah AT, Das PP (2017) Highly efficient catalytic reductive degradation of various organic dyes by Au/CeO_2-TiO_2 nano-hybrid. J Chem Sci129:81-93. doi:10.1007/s12039-016-1203-0

Saravanan R, Sacari E, Gracia F, Khan MM, Mosquera E, Gupta VK (2016) Conducting PANI stimulated ZnO system for visible light photocatalytic degradation of coloured dyes. J Mol Liq 221:1029-1033. https://doi.org/10.1016/j.molliq.2016.06.074

Segale L, Giovannelli L, Mannina P, Pattarino F (2016) Calcium alginate and calcium alginate-chitosan beads containing celecoxib solubilized in a self-emulsifying phase. Scientifica 2016:5062706. https://doi.org/10.1155/2016/5062706

Su Y, Yang Y, Zhang H, Xie Y, Wu Z, Jiang Y, Fukata N, Bando Y, Wang ZL (2013) Enhanced photodegradation of methyl orange with TiO_2 nanoparticles using a triboelectric nanogenerator. Nanotechnol 24:295401. doi: 10.1088/0957-4484/24/29/295401

Van Phu D, Duy NN, Lan NT, Du BD, Hien NQ (2014) Study on antibacterial activity of silver nanoparticles synthesized by gamma irradiation method using different stabilizers. Nanoscale Res Lett 9:1-5. https://doi.org/10.1186/1556-276X-9-162

Viswanathan B (2018) Photocatalytic degradation of dyes: An overview. Curr Catal 7:99-121. doi: 10.2174/2211544707666171219161846

Wang S, Vincent T, Faur C, Guibal E (2016) Alginate and algal-based beads for the sorption of metal cations: Cu (II) and Pb (II). Int J Mol Sci 17:1453-1478. doi: 10.3390/ijms17091453

Wang Y, Guo JS (2015) Catalyzed oxidative degradation of methyl orange over Au catalyst prepared by ionic liquid-polymer modified silica. IOP C Ser Mater Sci Eng 87:012019. doi:10.1088/1757-899X/87/1/012019

Wu HY, Jian WJ, Dang HF, Zhao XF, Zhang LZ, Li JH (2017) Hierarchical Ag-ZnO microspheres with enhanced photocatalytic degradation activities. Pol J Environ Stud 26:871-880. DOI: https://doi.org/10.15244/pjoes/65363

Zeynizadeh B, Behyar T (2005) Fast and efficient method for reduction of carbonyl compounds with NaBH4/wet SiO_2 under solvent free condition. J Braz Chem Soc 16:1200-1209. https://doi.org/10.1590/S0103-50532005000700018

Zha Y, Wang Y, Liu S, Liu S, Yang Y, Jiang H, Zhang Y, Qi L, Wang H (2018) Adsorption characteristics of organics in the effluent of ultra-short SRT wastewater treatment by single-walled, multi-walled, and graphitized multi-walled carbon nanotubes. Sci Rep 8:17245-17257. DOI:10.1038/s41598-018-35374-8

Zhang F, Wang X, Liu H, Liu C, Wan Y, Long Y, Cai Z (2019) Recent advances and applications of semiconductor photocatalytic technology. Appl Sci 9:2489-2532. https://doi.org/10.3390/app9122489

Zheng Y, Cao L, Xing G, Bai Z, Huang J, Zhang Z (2019) Microscale flower-like magnesium oxide for highly efficient photocatalytic degradation of organic dyes in aqueous solution. RSC Adv 9:7338-7348. https://doi.org/10.1039/C7CP07984B

Figures

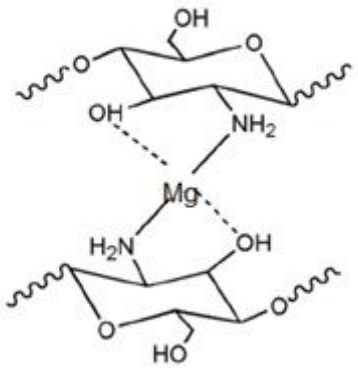

Figure 1

Chitosan chelation by Mg2+

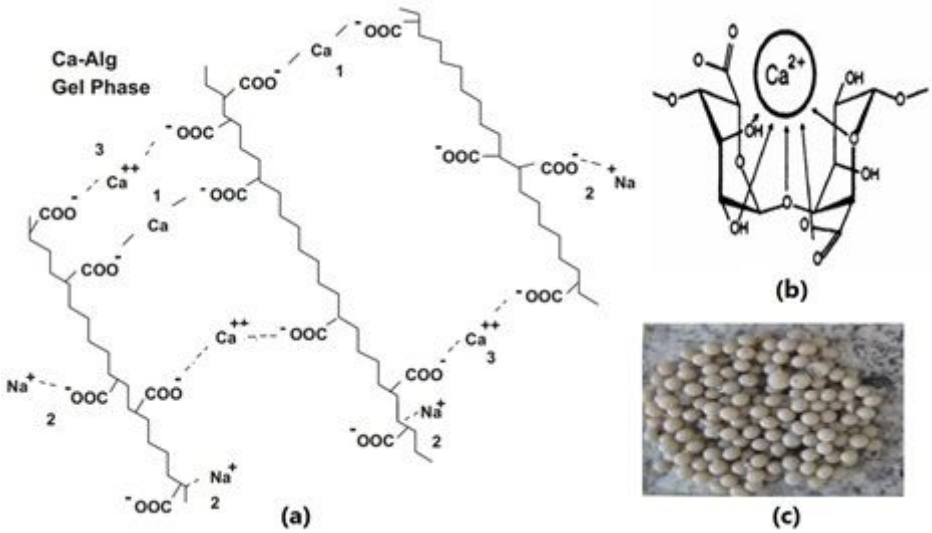

Figure 2

[a]: Schematic diagram of calcium alginate beads. (1) calcium bound; (2) Na+ ions that remains in the gel to balance the unoccupied carboxyl groups; (3) free, unbound Ca+2 ions in the gel phase; dashed lines represent electrostatic interaction between NP and unoccupied carboxyl groups, [b] Calcium alginate–egg-box structure, and [c] A photograph of ALG-(MgO/CS) beads

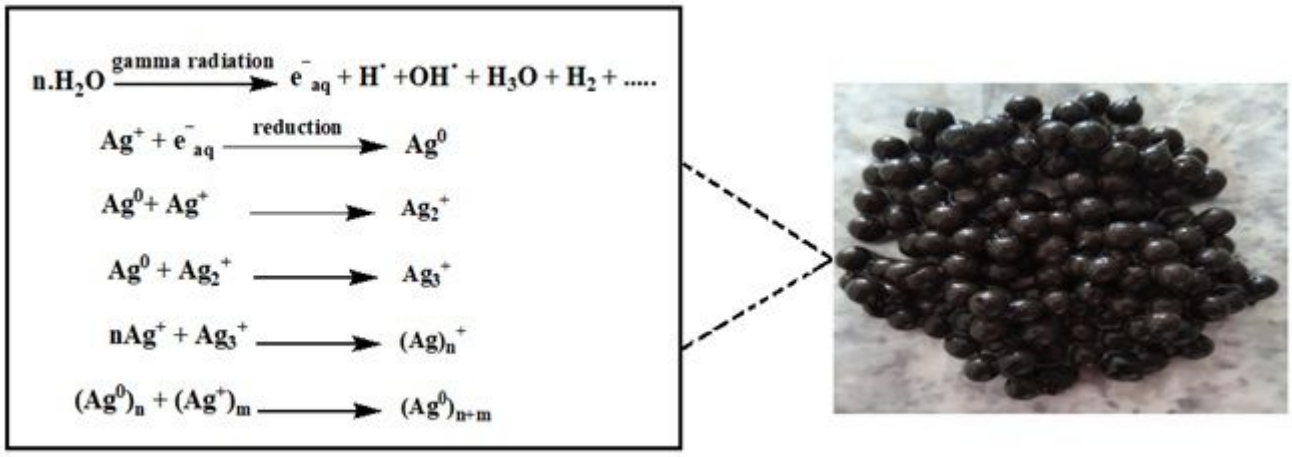

Figure 3

Schematic illustration of AgNPs formation under the reducing action of gamma radiation and a photograph of Ag/ALG-(MgO/CS)

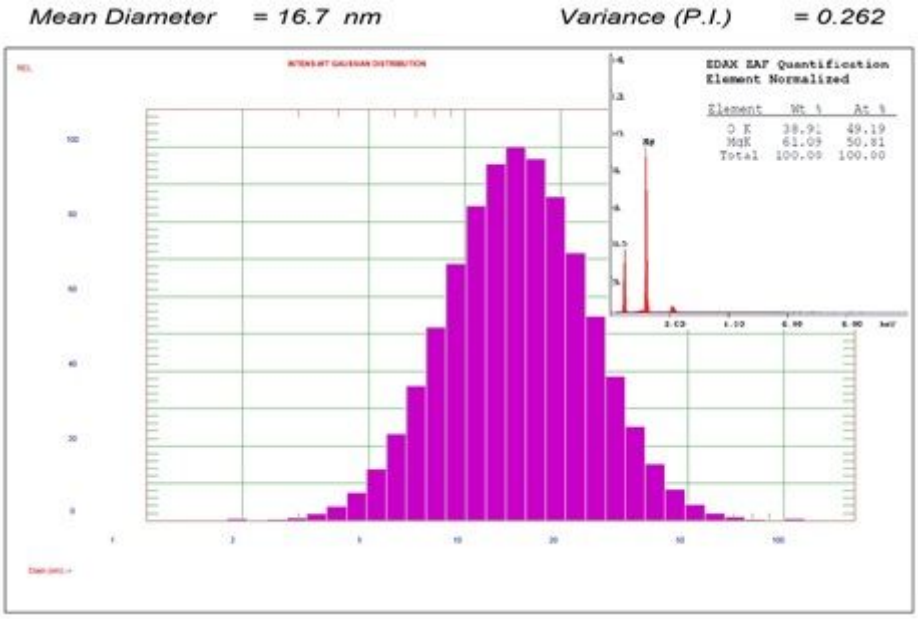

Figure 4

DLS intensity weighted distribution of as-synthesized MgO NPs. The inset represents EDX spectrum

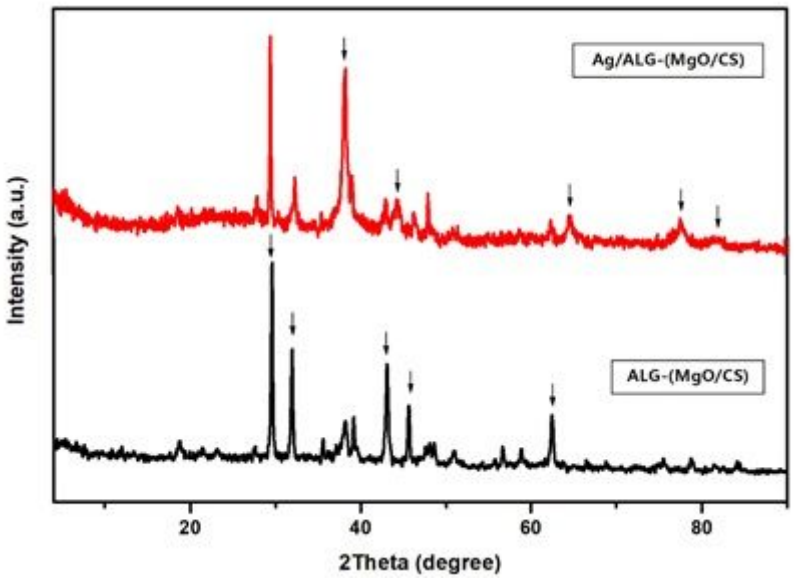

Figure 5

XRD patterns of ALG-(MgO/CS) and Ag/ALG-(MgO/CS)

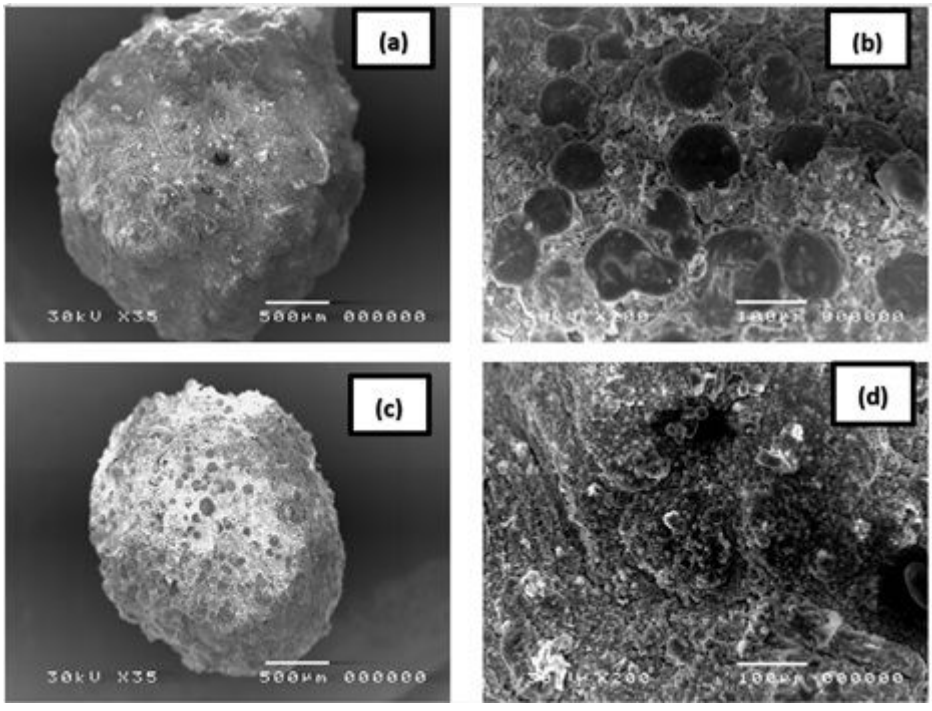

Figure 6

SEM micrographs of: (a, b) ALG-(MgO/CS); (c, d) Ag/ALG-(MgO/CS). Magnification was 35 and 200x for (a, c) and (b, d) respectively

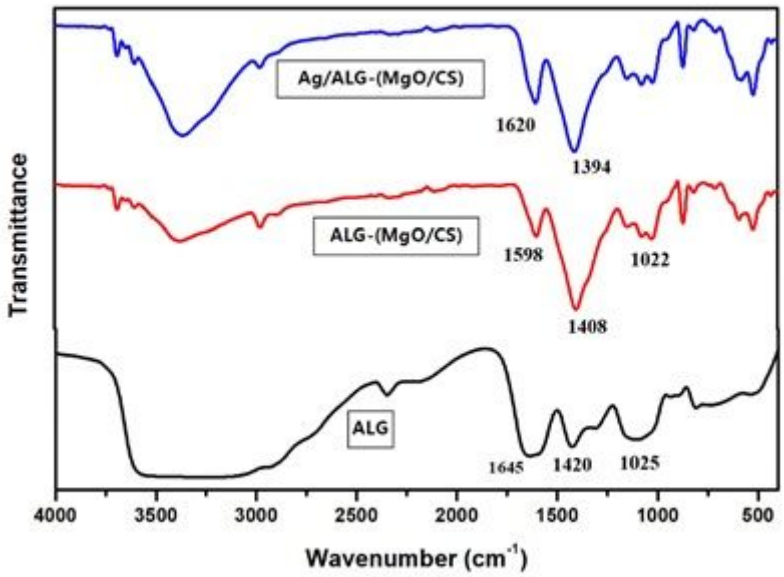

Figure 7

FTIR spectra of ALG, ALG-(MgO/CS) and Ag/ALG-(MgO/CS)

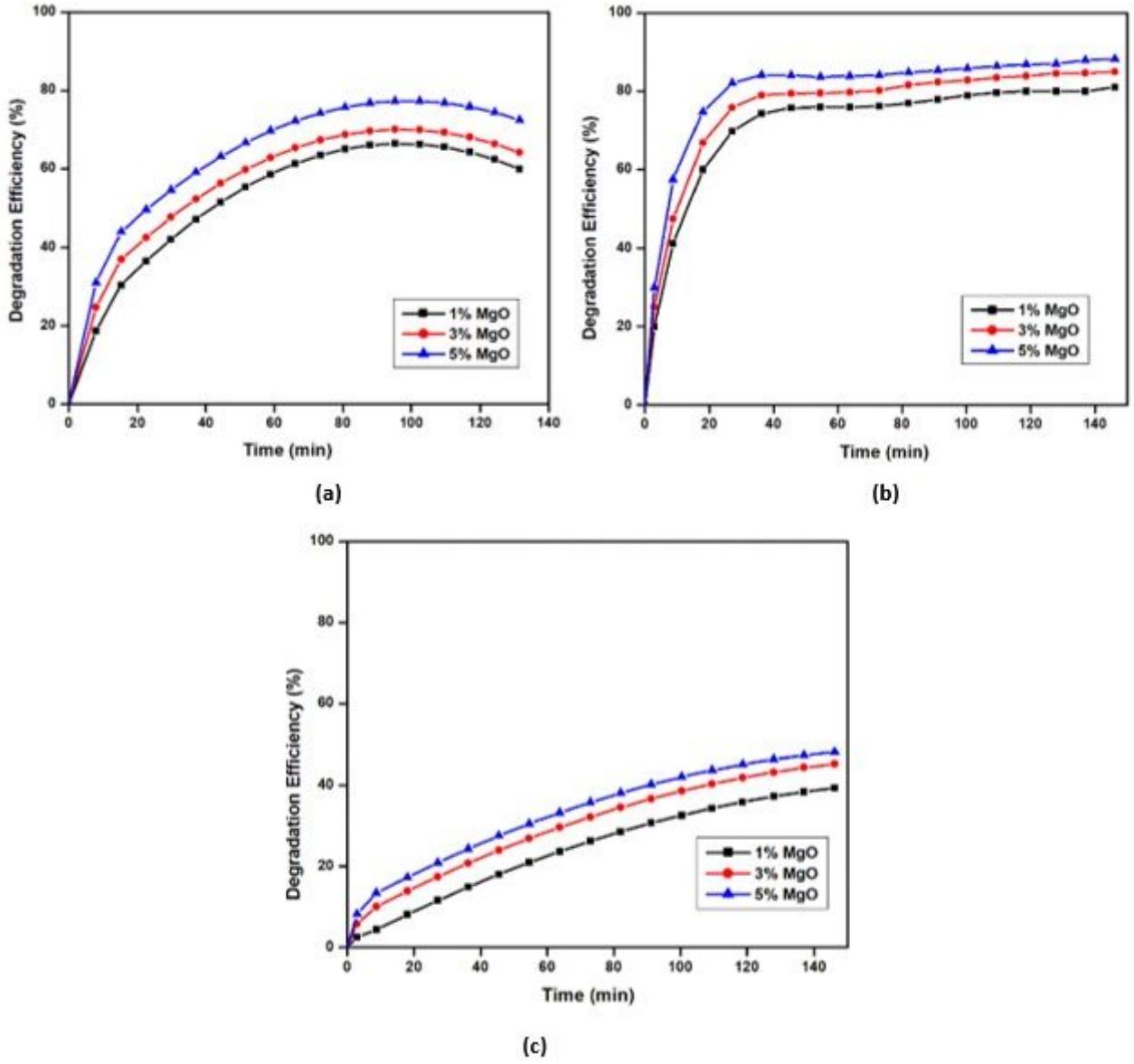

Figure 8

Relation between the degradation efficiency of ALG-(MgO/CS) beads and time through different MO concentration (a) 15 ppm; (b) 30 ppm and (c) 60 ppm. The study parameter was MgO concentration (1, 3 and 5%)

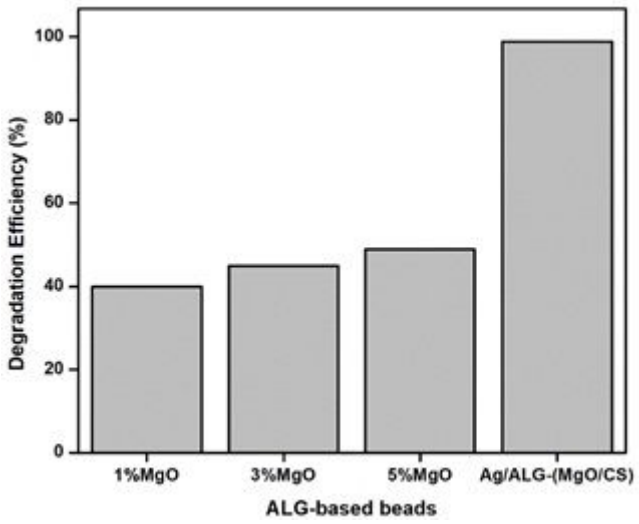

Figure 9

Degradation efficiency of 60 ppm MO by ALG-(MgO/CS) beads with different MgO concentrations and Ag/ALG-(MgO/CS) beads

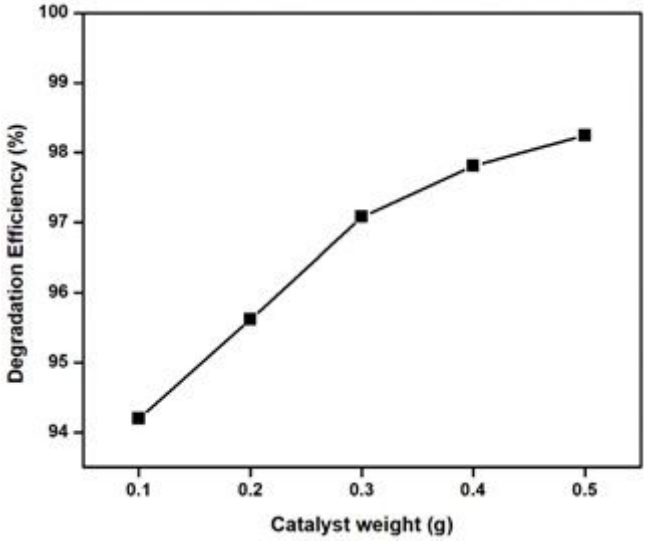

Figure 10

Relation between the degradation efficiency of Ag/ALG-(MgO/CS) beads and catalyst weight at MO concentration 60 ppm

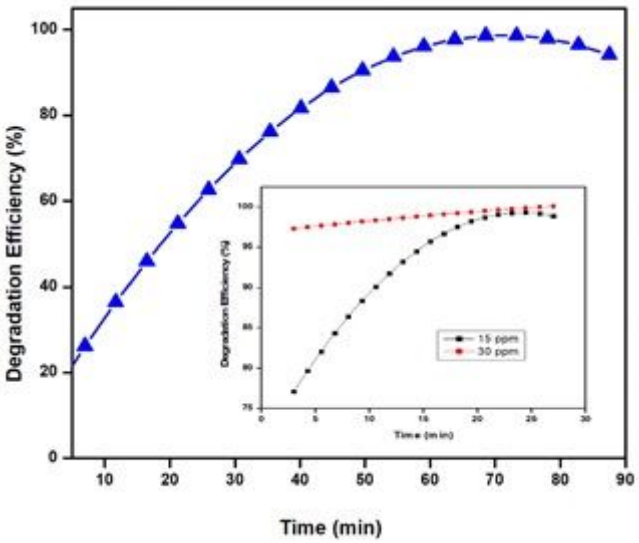

Figure 11

Relation between the degradation efficiency of Ag/ALG-(MgO/CS) beads and time at MgO concentration; 5% and MO concentration; 60 ppm. The inset represents the degradation efficiency at MO concentration; 15 and 30 ppm

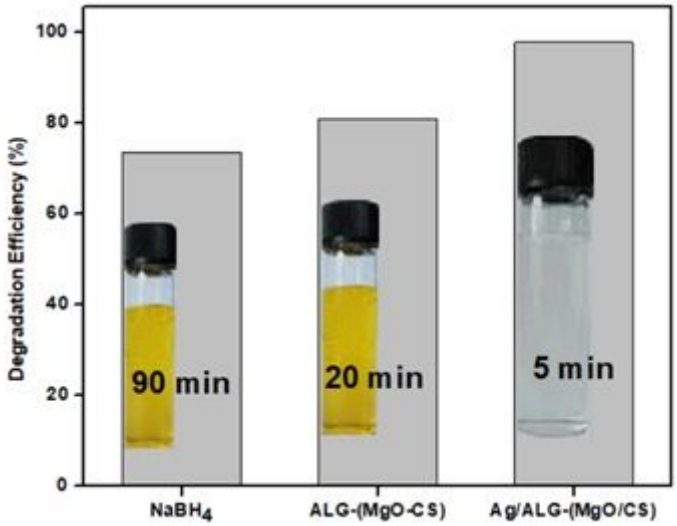

Figure 12

Comparison infographic of NaBH4 and the as-synthesized catalytic beads

Supplementary Files

This is a list of supplementary files associated with this preprint. Click to download.

- GraphicalAbstract.jpg